JGR Space Physics

RESEARCH ARTICLE
10.1029/2020JA027869

The Solar Wind Density Control on the Prompt Penetration Electric Field and Equatorial Electrojet

B. Nilam[1], S. Tulasi Ram[1], K. Shiokawa[2], N. Balan[3], and Q. Zhang[3]

[1]Indian Institute of Geomagnetism (IIG), Navi Mumbai, India, [2]Institute for Space-Earth Environmental Research (ISEE), Nagoya University, Nagoya, Japan, [3]Institute of Space Science, Shandong University, Weihai, China

Key Points:

- Prompt eastward/westward electric field disturbances of ~20 min are observed on dayside/nightside in response to sharp density enhancements
- Similar PPEF disturbances of opposite polarity are observed in response to sharp decreases in the solar wind density
- The polarity of PPEF/EEJ disturbances depends mainly on the local time without any dependency on the polarity of IMF *Bz* and *By*

Correspondence to:
S. T. Ram,
tulasi@iigs.iigm.res.in

Citation:
Nilam, B., Ram, S. T., Shiokawa, K., Balan, N., & Zhang, Q. (2020). The solar wind density control on the prompt penetration electric field and equatorial electrojet. *Journal of Geophysical Research: Space Physics*, *125*, e2020JA027869. https://doi.org/10.1029/2020JA027869

Received 31 JAN 2020
Accepted 17 JUL 2020
Accepted article online 11 AUG 2020

Abstract Prompt penetration of convection/overshielding electric fields to equatorial and low latitudes during the southward/northward turnings of interplanetary magnetic field (IMF *Bz*) have been widely studied in the literature. The other types of penetration electric fields due to sudden changes in the solar wind dynamic pressure, IMF *By* and during the onset of substorms have also been recently reported. In this paper, we present the exclusive role of solar wind density changes on the prompt equatorial electric field disturbances using the long-term observations of equatorial electrojet (EEJ) from the Indian sector. In response to the sharp increases in the solar wind density, prompt increases/decreases in the EEJ indicating the eastward/westward prompt penetration electric field (PPEF) of ~20 min periods have been consistently observed on the dayside/nightside. The prompt equatorial electric field disturbances of the opposite polarity have also been observed when the density decreases sharply. Further, the polarity of these PPEF disturbances does not show any clear dependency on the direction of IMF *Bz* and *By*. This paper is the first report with a statistically significant number of observations on the characteristics of equatorial electric field disturbances in response to the sudden enhancements/decreases in the solar wind density alone on both dayside and nightside. The underlying physical mechanisms for the prompt equatorial electric field disturbances have been discussed in light of enhanced high-latitude convection and additional field-aligned currents due to sudden enhancement of solar wind density.

1. Introduction

Interaction of terrestrial magnetosphere with the incoming supersonic solar wind plasma is a continuous process. In addition to the continuously streaming-in ambient solar wind, the transient and recurrent structures in the solar wind during the disturbed space weather periods often cause enhanced solar wind-magnetosphere interactions and consequent disturbances in the Earth's near-space environment. A large amount of energy and momentum is transferred from solar wind to the coupled magnetosphere-ionosphere-thermosphere system. The complex flows of plasma and open field magnetic flux in the magnetosphere and ionosphere develops a variety of current systems and electric fields. Of the particular interest here is the high-latitude convection electric field due to solar wind-magnetosphere dynamo which penetrates promptly to the equatorial and low-latitudes, known as prompt penetration electric field (PPEF) (Kikuchi et al., 1996, 2000; Nishida, 1968; Senior & Blanc, 1984). Under southward orientation of interplanetary magnetic field (IMF *Bz*), the enhanced high-latitude dawn-to-dusk convection electric field induces eastward/westward PPEF disturbances in the dayside/nightside ionosphere, respectively (Fejer, 1991; Fejer & Scherliess, 1997; Kelley et al., 1979). Westward shielding electric fields will soon develop in the inner magnetosphere due to azimuthal gradient of plasma pressure, known as shielding electric fields. During the northward turning of IMF *Bz*, the termination of convection fields leads to the domination of shielding electric fields in the inner magnetosphere, a condition known as overshielding, which causes westward/eastward PPEF disturbances in the dayside/nightside ionosphere, respectively (Kikuchi et al., 1996, 2003; Rastogi & Patel, 1975). The equatorial electric field disturbances due to prompt penetration of convection/overshielding electric fields under southward/northward IMF *Bz* conditions, respectively, and the resultant modifications in the equatorial ionosphere have been widely studied in the literature (e.g., Abdu et al., 1995; Basu et al., 2001, 2005; Fejer & Scherliess, 1997; Kelley et al., 1979; Tulasi Ram et al., 2008, 2012, 2015, and references therein).

During the recent past, a few other types of prompt equatorial electric field disturbances were also reported which are not associated with any changes in the orientation of IMF *Bz*. Kelley and Makela (2002) and Chakrabarty et al. (2017) have reported the prompt electric field disturbances in the equatorial ionosphere in response to sharp changes in dawn-to-dusk component of IMF (i.e., IMF *By*) under steady IMF *Bz* conditions. On the other hand, prompt electric field disturbances of both westward and eastward polarities have been observed in the dayside equatorial ionosphere during the onset of substorms (Ebihara et al., 2014; Hashimoto et al., 2017; Huang, 2012; Huang et al., 2004; Kikuchi et al., 2000; Sastri et al., 2001; Venkatesh et al., 2017). Further, prompt equatorial electric field perturbations in response to the sudden enhancement in the solar wind dynamic pressure (P_{Dyn}) have also been reported during the geomagnetic sudden commencement (SC) (Araki, 1977; Kikuchi et al., 2001; Sastri et al., 1993) as well as isolated events of P_{Dyn} enhancements (Huang et al., 2008; Rout et al., 2016). More recently, Tulasi Ram et al. (2019) have demonstrated the three episodes of prompt equatorial electric field disturbances of opposite polarities on dayside and nightside due to the sudden changes in P_{Dyn}, IMF *By*, and onset of a substorm under the steady southward IMF *Bz* conditions during the St. Patrick's Day storm of 17 March 2015.

According to the physical model of Araki (1994), the low-latitude geomagnetic field exhibits a short preliminary impulse (~1 min), a main impulse (~10 min), and a step-like increase in response to the P_{Dyn} enhancement during the geomagnetic SC. While the preliminary impulse (PI) and main impulse (MI) are attributed to the increased field-aligned currents, the step-like increase corresponds to the increased magnetopause (Chapman-Ferraro) currents (Araki, 1994; Kikuchi & Araki, 1985). Araki (1994) and Kikuchi et al. (2001) have shown that the PI is primarily due to additional field-aligned currents flows into (out of) ionosphere in the afternoon (morning) sector driven by fast Alfven mode compressional hydromagnetic wave and causes disturbance dusk-to-dawn polar electric fields. The MI is attributed to the enhanced dawn-to-dusk convection electric field, which is induced in order to adjust the new compressed state of magnetosphere, and the associated field-aligned currents flows into the dawn and out of dusk ionosphere. The additional field-aligned currents during PI and MI lead to the disturbance polar (DP) dusk-to-dawn and dawn-to-dusk electric fields, respectively, which promptly penetrates to the equatorial and low latitudes as observed from ground-based magnetometer (Kikuchi, 1986; Kikuchi et al., 2001) and HF Doppler radar (Kikuchi et al., 1985; Sastri et al., 1993). Later, Huang et al. (2008) have shown the simultaneous enhancement of ionospheric convection at high latitudes using Super Dual Auroral Radar Network (SuperDarn) HF radars and vertical $E \times B$ ion drift at equatorial latitudes using Jicamarca Incoherent Scatter Radar on dayside in response to the sharp enhancements of P_{Dyn}. Yuan and Deng (2007) have also shown the variations of PPEF in the equatorial ionosphere due to the changes in the P_{Dyn}.

Although the above studies show the role of P_{Dyn} on the prompt ionospheric electric field disturbances at equatorial latitudes, the exclusive role of solar wind density variations on the PPEF at equatorial ionosphere has not been studied extensively. Wei et al. (2012) have reported that the cross polar cap potential (CPCP) is decoupled from the interplanetary electric field and modulates coherently with the solar wind density under the polar cap saturation conditions. Recently, Rout et al. (2016) have presented a case study of penetration electric fields due to density pulse under steady solar wind velocity and northward IMF *Bz* conditions on 22 January 2012. They have shown the prompt elevation of *F*2 layer peak height (hmF2) and modest increase of EEJ indicating the eastward PPEF on dayside in response to the solar wind density increase. Therefore, in order to shed further light on role of solar wind density, we investigate and present the prompt equatorial electric field disturbances on both dayside and nightside in response to the exclusive changes in the solar wind density under steady solar wind velocity and interplanetary dawn-to-dusk electric field conditions (IEFy).

2. Data

The Equatorial Electrojet (EEJ) variations over a long period (2001–2018) over Indian sector derived from two ground-based magnetometers at an equatorial station, Tirunelveli (TIR, 8.7°N, 77.8°E, 0.8°N dip latitude) and an off-equatorial station, Alibag (ABG, 18.6°N, 72.9°E, 10.5°N dip latitude) have been considered in this study. The baseline values of the horizontal (*H*) component of the geomagnetic field at each station are computed by averaging the local midnight values of five internationally quiet days in every month. The baseline values of each month are then subtracted from *H* component values at each station to derive

the ΔH variations. The difference of ΔH values between Tirunelveli (equatorial station) and Alibag (off-equatorial station), that is, (EEJ $= \Delta H_{\mathrm{Tir}} - \Delta H_{\mathrm{Abg}}$) represents the EEJ strength which is a proxy to the equatorial zonal electric field (Anderson et al., 2002; Kane, 1974; Rastogi, 1977; Reddy, 1989). The high-latitude convection map data from the SuperDARN have been considered to see the changes in the high-latitude dawn-to-dusk convection electric fields in response to the sudden changes in the solar wind density. Further, the solar wind observations (velocity, density, IMF *Bz*, and *By*) at 1-min resolution which are time shifted to bow shock nose were obtained from NASA's OMNI Space Physics Data Facility (https://omniweb.gsfc.nasa.gov/ow_min.html).

3. Results

In order to study the explicit role of solar wind density on PPEF at equatorial latitudes, the events of sharp increases/decreases in the solar wind density without significant changes in the other solar wind parameters such as velocity (V), interplanetary electric field (IEFy $= -V \times$ IMF *Bz*), interplanetary magnetic field components (IMF *Bz* and *By*) are selected from the long-term solar wind observations during 2001 to 2018. The selection criteria include (i) a sharp increase or decrease of solar wind density with an absolute change ($|\Delta N|$) greater than 8 particles/cm^3 at an average rate of change greater than 2 particles/cm^3/min, (ii) the changes in the solar wind velocity and interplanetary electric field must be small during the 10-min period from the onset of density change, that is, ($|\Delta V|_{10\mathrm{min}} < 50$ km/s and$|\Delta \mathrm{IEFy}|_{10\mathrm{min}} < 2$ mV/m) to avoid the PPEF effects during SC and due to changes in the IEFy (which is a product of velocity and IMF *Bz*). Similarly, (iii) the changes in the IMF *Bz* and *By* within a 10-min period from the onset of density change must be small, that is, $|\Delta Bz|_{10\mathrm{min}}$ and $|\Delta By|_{10\mathrm{min}} < 10$ nT. In addition, (iv) the density variations during the previous 30 min (preepoch) and after 30 min (postepoch) of the event should be small, that is, the standard deviation of density fluctuations during preepoch and postepoch periods must be smaller than 3 particles/cm^3. This condition is applied to ensure the quiescence during preepoch/postepoch periods and to select the isolated events of sharp step-like density changes by avoiding the too fluctuating and oscillatory variations in the density. Although we have searched over long-term observations from 2001–2018, the strict selection criteria (i)--(iv) above and some gaps in the data give rise to a total of 68 events of sudden step-like density increases and 70 events of sudden density decreases without any significant changes in the other solar wind parameters.

3.1. PPEF Due to Solar Wind Density Enhancement

Figure 1 shows two typical events of sharp density enhancements while the other solar wind parameters are more or less steady. The panels from top to bottom in Figure 1 show the variations in solar wind density (N), velocity (V), dawn-dusk interplanetary electric field (IEFy), IMF *Bz* (black) and *By* (red), ΔH variations at Tirunelveli (black) and Alibag (red), and the EEJ, respectively, as a function of epoch time in minutes. The left- and right-hand side panels of (Figure 1) correspond to the events that occurred during local daytime and nighttime periods over the Indian sector, respectively. The vertical blue dashed line indicates the time of sharp increase in solar wind density. It can be seen from this figure that the solar wind density exhibits a sharp increase of ~10 particles/cm^3 at zero epoch time without any significant change in the velocity. The IEFy exhibits only a few small fluctuations due to fluctuations in the IMF *Bz*. On the other hand, the ΔH variations from the two ground-based magnetometers at Tirunelveli and Alibag exhibit sharp increases concurrently with the density enhancements. Further, the increase in the ΔH at the equatorial station (TIR) is significantly large compared to that at the off-equatorial station (ABG). Accordingly, the EEJ (EEJ $= \Delta H_{\mathrm{Tir}} - \Delta H_{\mathrm{Abg}}$) exhibits a sharp increase of ~10 nT indicating the eastward PPEF at the equatorial latitudes on the dayside. It should be emphasized here that the observed eastward PPEF (increase in EEJ) on dayside is exclusively due to the sharp increase in solar wind density without any significant changes in the other solar wind parameters during this epoch. Therefore, this is an impeccable example of eastward PPEF on dayside caused exclusively by sharp enhancement in solar wind density.

Figure 1 (right panel) shows another example of sharp density enhancement that occurred during the local nighttime over the Indian sector. It can be seen from this figure that the density exhibits a sharp increase of ~10 particles/cm^3 at zero epoch time without any significant changes in the velocity and IEFy except for small fluctuations. The IMF *Bz* and *By* also do not exhibit any significant changes during this period except for a few minor fluctuations. The ΔH variations at both TIR and ABG also exhibits sharp enhancements

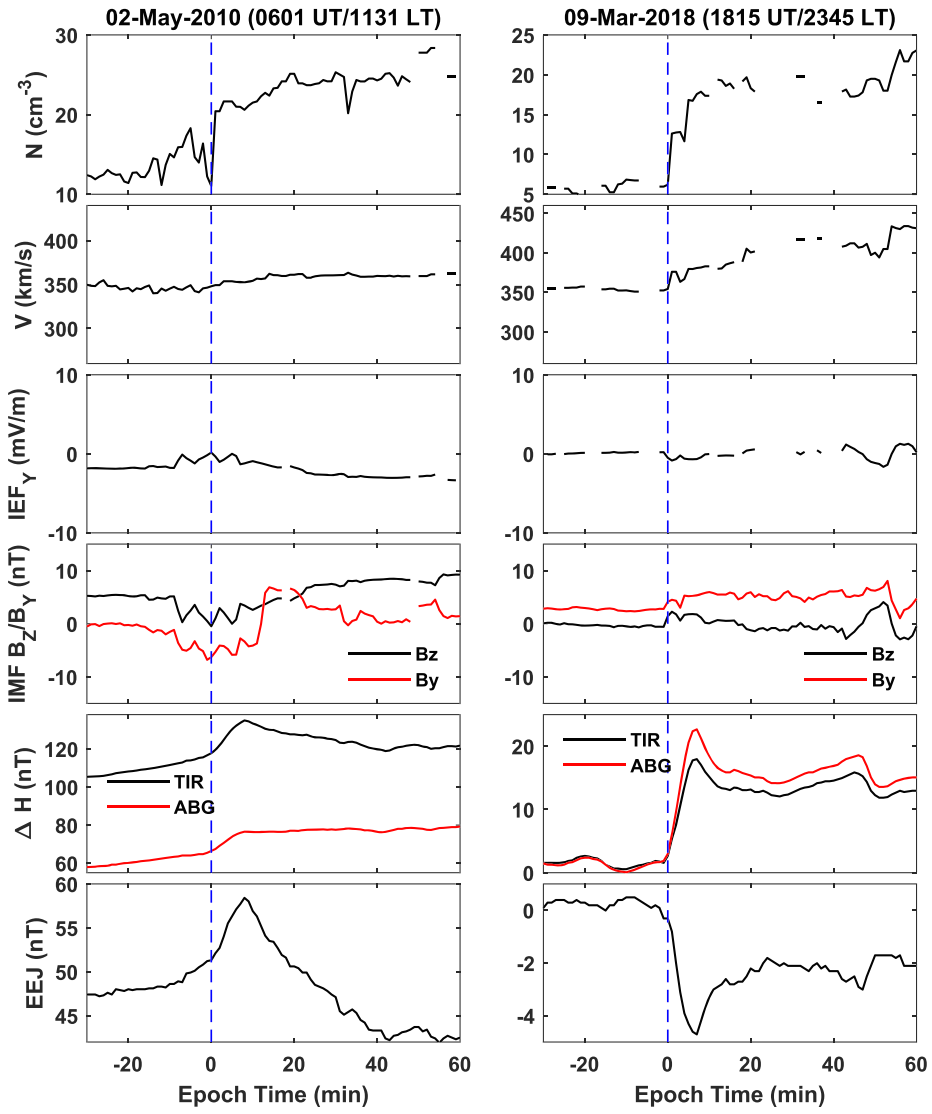

Figure 1. Two typical examples of sharp solar wind density enhancements occur at local daytime (left panels) and nighttime (right panels) and corresponding changes in the geomagnetic field (ΔH) and equatorial electrojet (EEJ). The panels from top to bottom present the variations of solar wind density, velocity, IEFy, IMF *Bz* (black), *By* (red), Δ*H* at Tirunelveli (black) and Alibag (red curve), and the equatorial electroJet (EEJ), respectively. The vertical blue dashed line indicates the time of sharp density enhancement (zero epoch time).

concurrently with the density enhancements; however, the Δ*H* variation at TIR (equatorial station) is smaller compared to that at ABG (off-equatorial station) during this nighttime event. As a result, the EEJ exhibits a sharp decrease of ~4 nT indicating the westward PPEF on the nightside induced by the enhancement in solar wind density. It should be noted that the ionospheric conductivity on the nightside being very small, the variations in EEJ current due to PPEF is very small on the nightside compared to the dayside observations (Rastogi et al., 1996) (note the difference in the *y* axis scales for EEJ between the left and right panels). Nevertheless, the Figure 1 (right panel) presents a clear example of westward PPEF on the nightside induced by the solar wind density enhancement exclusively.

In order to further examine the changes in the high-latitude convection patterns in response to the sudden increase in solar wind density, the SuperDARN convection maps from the Northern Hemisphere are presented in Figure 2 for the same two events presented in Figure 1. The top panels show the convection maps 10 min before the onset of sharp density enhancement. The middle and bottom panels show the convection

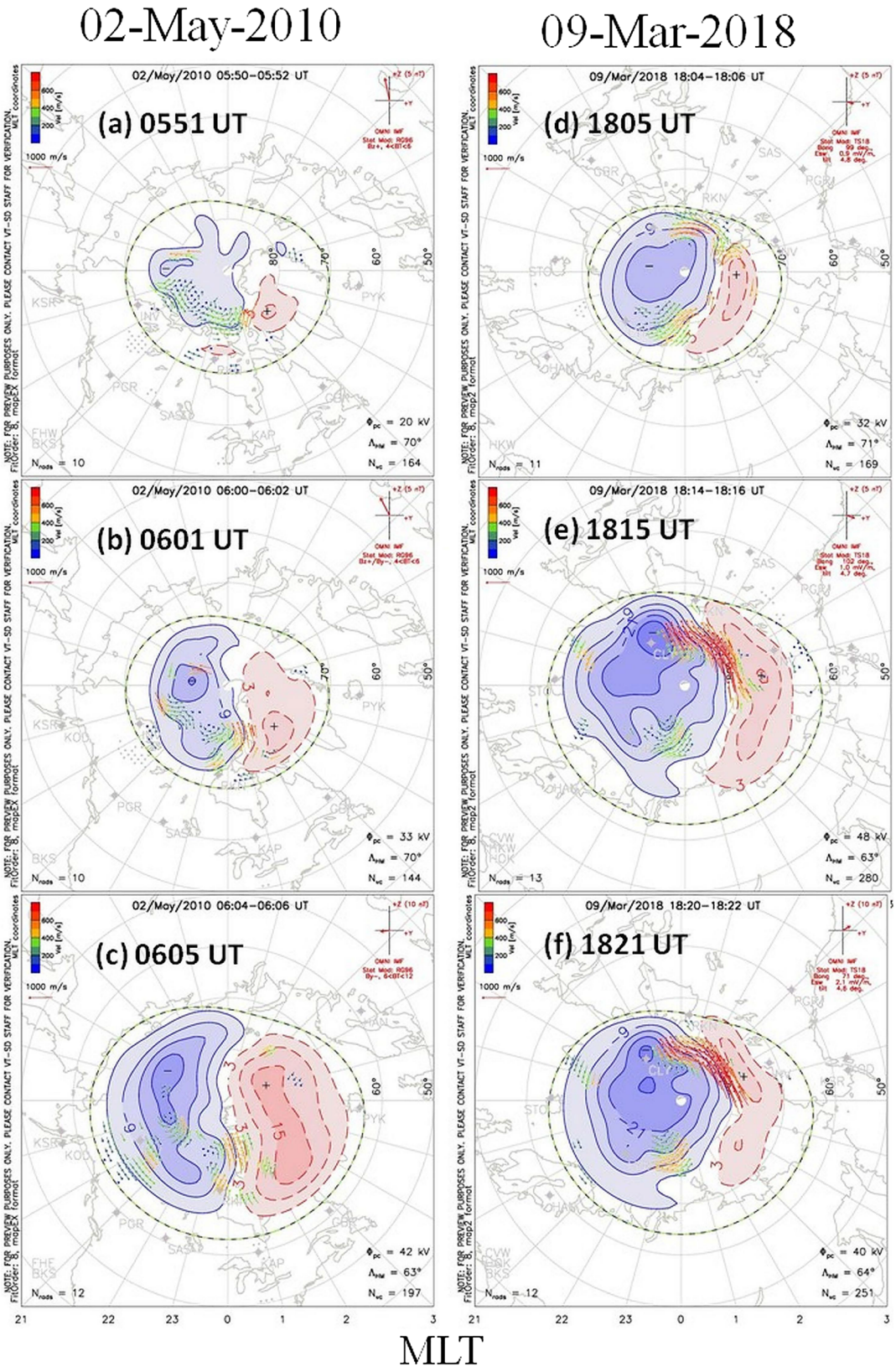

Figure 2. The northern high-latitude convection maps constructed from the SuperDARN HF radar network observations during the sharp density enhancement events presented in Figure 1. (a) and (d) correspond to 10 min prior to the density enhancement. (b) and (e) correspond to the time of density enhancement. (c) and (f) correspond to ~4–6 min after the density enhancement when the peak electrojet disturbances observed.

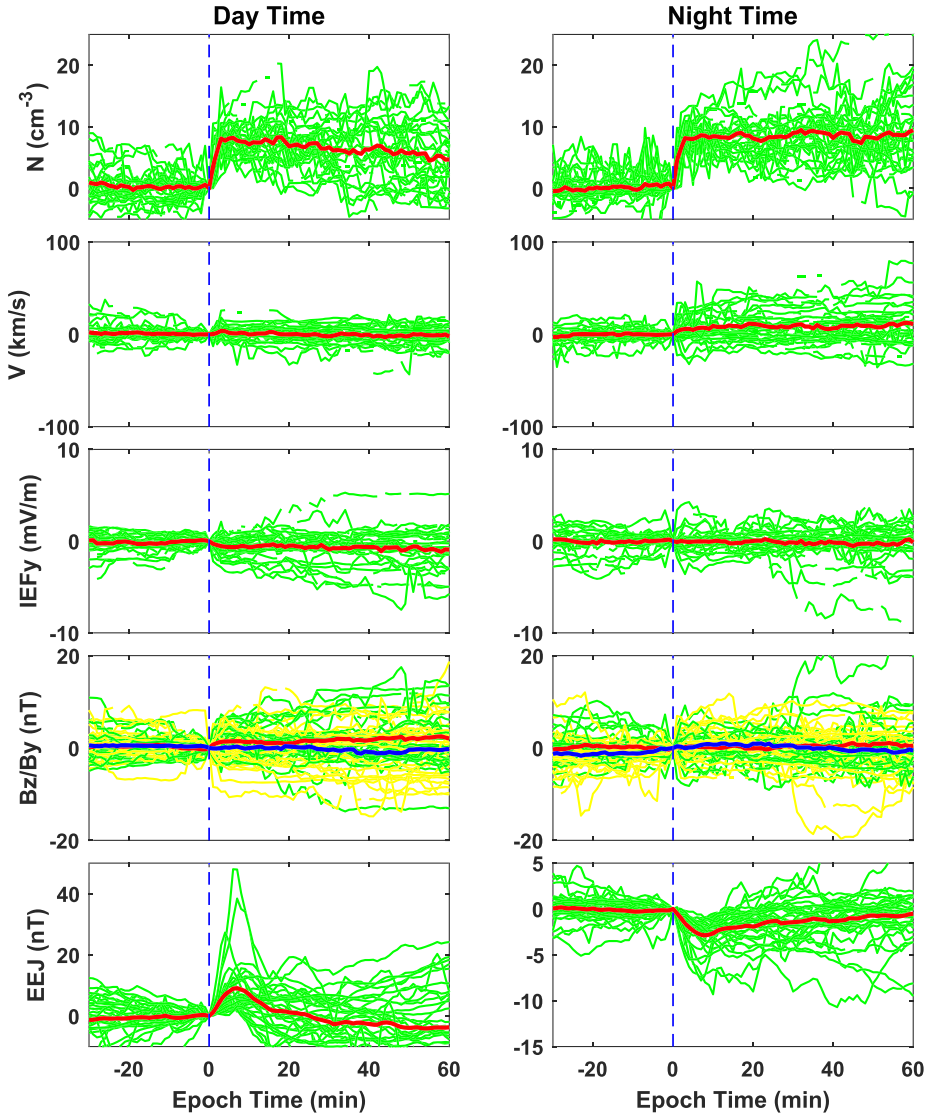

Figure 3. Superposed epoch analysis of sharp solar wind density enhancements and the corresponding changes in the equatorial electroJet (EEJ) during daytime (left panels) and nighttime (right panels). The panels from the top to bottom presents temporal variation of solar wind density, velocity, interplanetary electric field (IEFy), IMF *Bz* (green), *By* (yellow), and the equatorial electroJet (EEJ), respectively. The vertical blue line in all the panels represent the time of sharp enhancement in density (zero epoch time).

maps "at the time" and "~4–6 min after" the sharp density enhancement, respectively. As can be seen from these figures (Figure 2), the high-latitude dawn-to-dusk convection field increases noticeably with the increase in solar wind density during both events. The Indian sector happens to be on the noonside during the first event (left panels) and on the nightside during the second event (right panels), thus, witnessed eastward and westward PPEF perturbations, respectively, as shown in the bottom panels of Figure 1.

With a view to statistically establish the solar wind density role on the PPEF, the long-term observations of solar wind and EEJ during the period 2001–2018 were analyzed. As mentioned above, a total of 68 events of density enhancements without significant changes in velocity, IEFy, IMF *Bz* and *By* have been detected based on the selection criterion mentioned above. For example, Figure 3 shows the superposed epoch analysis of solar wind density enhancements and corresponding changes in the EEJ. The panels from top to

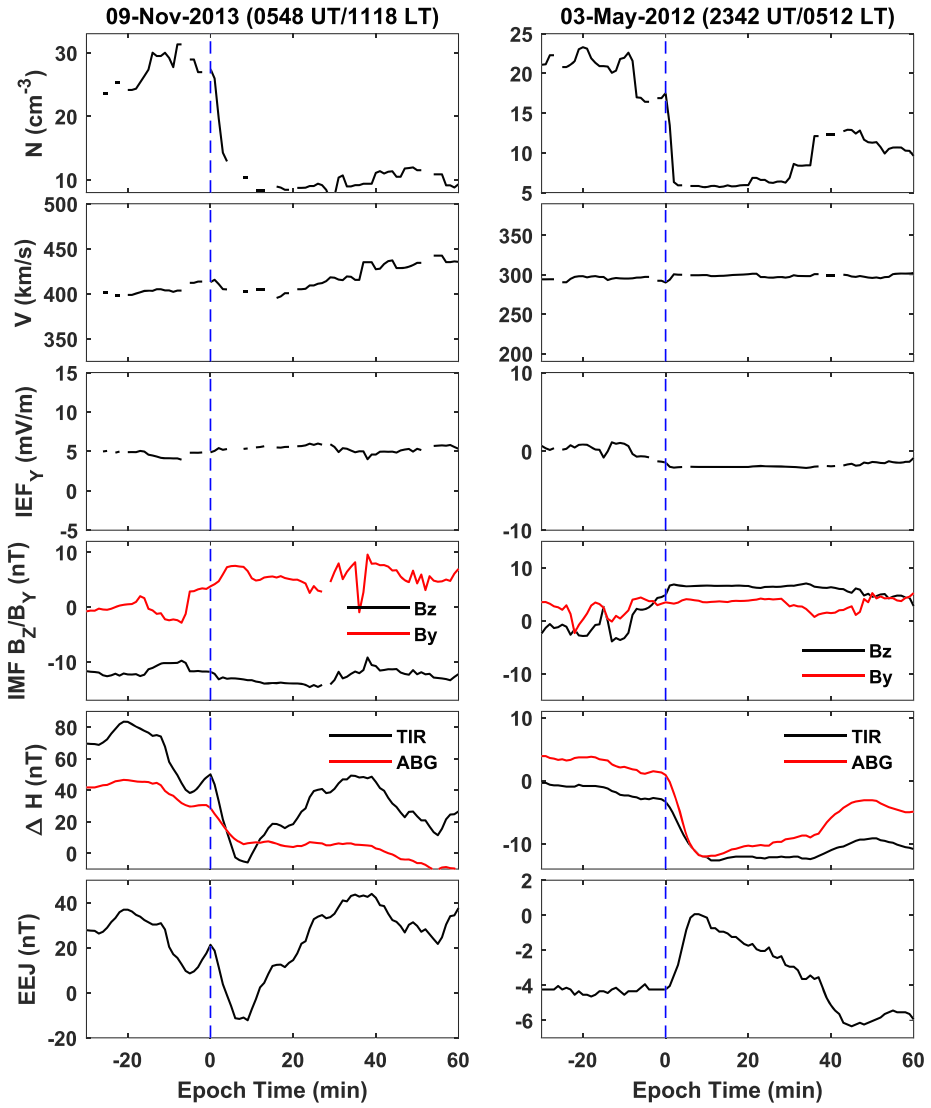

Figure 4. Same as Figure 1 except for the cases of sharp decrease in the solar wind density.

bottom show the variations of solar wind density, velocity, IEFy, IMF *Bz*/*By*, and EEJ, respectively. The vertical blue dashed line at zero epoch time indicates the time of sharp increase in solar wind density. The thin curves in green color represent the individual events, while the thick curve in red color represents the average variations in all the panels. The thin yellow curves in the fourth row panels indicate the IMF *By* variations and their average curves are shown in blue color. All the data shown in Figure 3 are the values relative to the corresponding parameters at zero epoch time. Therefore, Figure 3 actually presents the superposed variations in solar wind parameters and EEJ after the subtraction of respective constant values corresponding to the zero epoch time. The level shifting of data by subtracting the constant values is preferred (rather than traditional normalization), as this will allow the reader to observe the actual changes that occurred in the solar wind and EEJ. The left-hand side panels correspond to local daytime (06–18 LT) and right-hand side panels correspond to nighttime (18–06 LT) periods over the Indian sector.

From Figure 3, conspicuous enhancements (and decreases) in EEJ can be observed on dayside (and nightside) concurrently with the solar wind density enhancements. The opposite polarity of EEJ response during the daytime and nighttime is the convincing evidence for electric field disturbances in the equatorial ionosphere, as, in general, the ionospheric dawn-dusk electric field is curl-free. It may be recalled that the EEJ response during nighttime is significantly small (note the difference in *y* axis scale) due to very low

conductivity in the nightside ionosphere. Another interesting observation to be noted here is, while the density exhibits a step-like increase (and remains at high level for several tens of minutes), the EEJ responds in a spiky pulse-like variation with a duration of about ~20 min. The EEJ exhibits a quick increase (decrease) for about ~5–7 min on dayside (nightside) and recovers to background levels within ~20 min.

3.2. PPEF Due to Solar Wind Density Reduction

Using the same selection criterion mentioned above, the events of sharp decreases in solar wind density were also detected and corresponding changes in the EEJ are presented in this section. Figure 4 shows two typical examples of density reductions that occurred without any significant changes in the other solar wind parameters during local daytime (left panels) and nighttime (right panels) periods over the Indian sector. It can be observed from these figures that the ΔH variations exhibit decreases simultaneously with the density reductions on both dayside and nightside. However, the corresponding EEJ response (bottom panels) is prompt decrease and increase indicating the westward and eastward PPEF on the dayside and nightside, respectively. The high-latitude convection maps from the SuperDARN HF radars for the same events are shown in Figure 5. Noticeable decreases in the high-latitude convection field during both cases can be observed from these figures in response to the sudden decrease in the solar wind density (Figure 4).

Similar to Figure 3, Figure 6 shows the superposed epoch analysis of solar wind density reductions and the corresponding changes in the EEJ during both daytime (left panels) and nighttime (right panels) periods. It can be clearly observed from this figure that the EEJ exhibits a pulse-like negative and positive excursions of ~20 min periods on dayside and nightside, respectively, in response to the step-like decrease in solar wind density. Needless to say that the nightside response of EEJ is significantly small compared to dayside due to very low ionospheric conductivity during nighttimes.

4. Discussion

The EEJ, which is a proxy to the equatorial zonal electric field, found to exhibit prompt response to the sharp changes in the solar wind density. The important observations are briefly recalled here. (i) The EEJ exhibits prompt enhancements and decreases indicating the eastward and westward PPEF disturbances on dayside and nightside, respectively, in response to the sharp enhancements in the solar wind density. (ii) Further, the EEJ also exhibits westward and eastward PPEF signatures on dayside and nightside, respectively, in response to the sudden density reductions. (iii) While the solar wind density exhibits a step-like variation, the corresponding response in EEJ is a brief pulse-like variation of ~20 min period. (iv) The high-latitude dawn-to-dusk convection electric field also found to increase/decrease with the sharp increases/decreases in the solar wind density.

A series of changes would take place in the coupled magnetosphere-ionosphere system in response to sudden increase/decrease of solar wind density. The sharp increase/decrease of density results in sudden increase/decrease of solar wind dynamic pressure (P_{Dyn}). The increase of P_{Dyn} causes magnetosphere to compress and the magnetopause *stand-off distance* decreases (Pudovkin et al., 1998). Further, magnetopause currents would suddenly increase due to increased density. Both the magnetosphere compression and the magnetopause currents would lead to sudden increase in the geomagnetic field measured from the ground-based magnetometers (Araki, 1977, 1994). The sudden increases of ΔH values at both Tirunelveli and Alibag in Figure 1 (fifth row, left panels) represent these effects. However, the interesting observation to be noted here is that the ΔH increase at the equatorial station TIR (0.8° dip lat) is significantly higher than that at the off-equatorial station ABG (10.5° dip lat) on the dayside (Figure 1, left panels). On the other hand, the ΔH increase at TIR is smaller compared to that at ABG on the nightside (Figure 1, right panels). Since the effects of magnetosphere compression and magnetopause currents do not expect to exhibit such a significant latitudinal gradient within few (<10°) degrees apart (e.g., Kikuchi et al., 2001), the observed difference in the ΔH increase between TIR and ABG is mainly due to the additional currents flowing in the ionosphere. It is well known that the zonal current in the ionosphere is significantly enhanced over a narrow belt (±2–3°) of latitudes centered on equator due to Cowling effect (Hirono, 1952), known as equatorial electrojet, (Kane, 1974; Rastogi, 1977; Reddy, 1989). The EEJ is generally given as, EEJ $= \sigma_c\, E_x$, where E_x is the dawn-to-dusk electric field in the ionosphere and σ_c is the Cowling conductivity, a scalar quantity proportional to ionospheric Pederson and Hall conductivities which in turn are proportional to the ionospheric electron density. Hence, the sense of EEJ mainly depends on the E_x, while the magnitude of

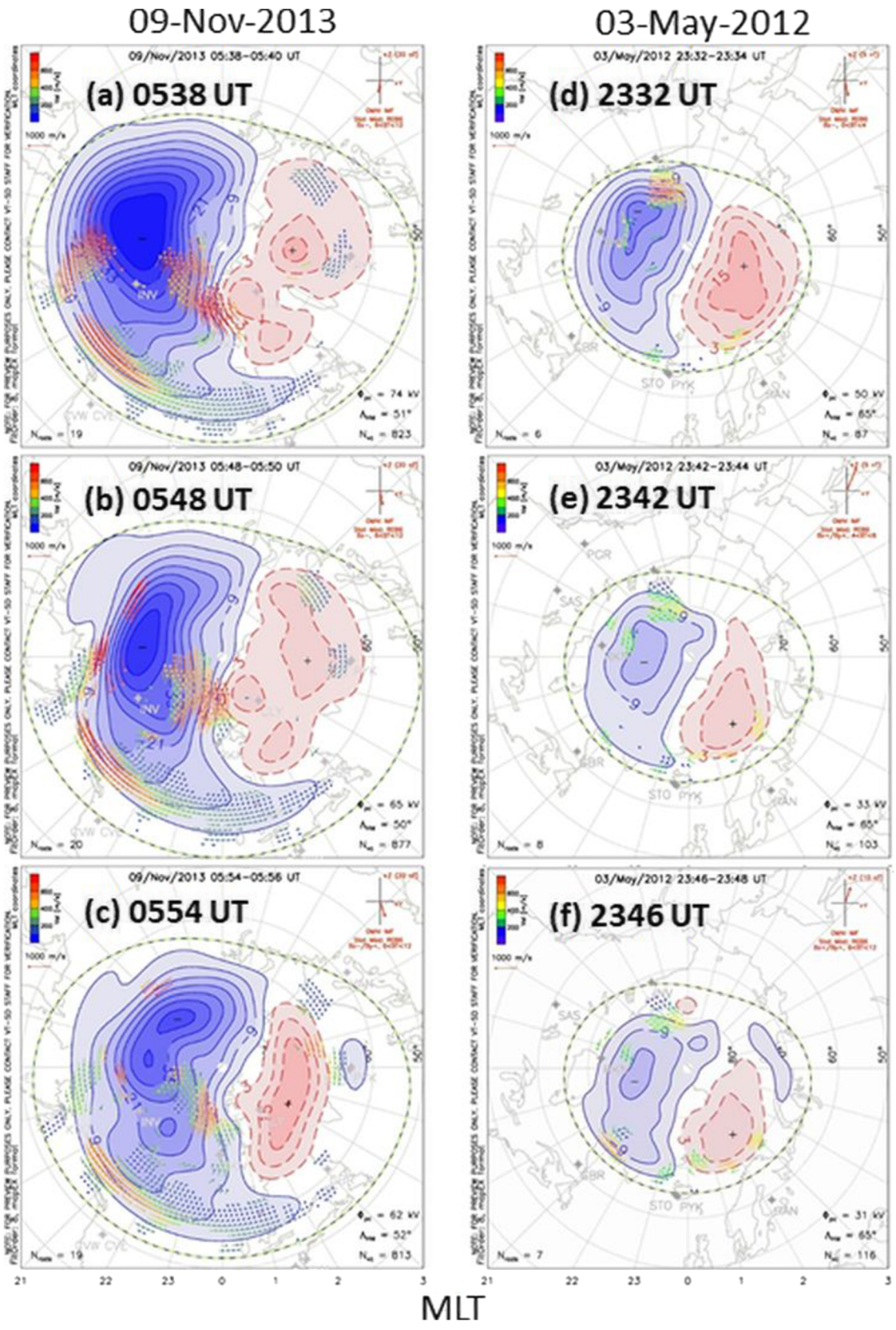

Figure 5. The northern high-latitude convection maps constructed from the SuperDARN HF radar network observations during the sharp density reduction events presented in Figure 4. (a) 0538 UT; (b) 0548 UT; (c) 0554 UT; (d) 2332 UT; (e) 2342 UT; (f) 2346 UT.

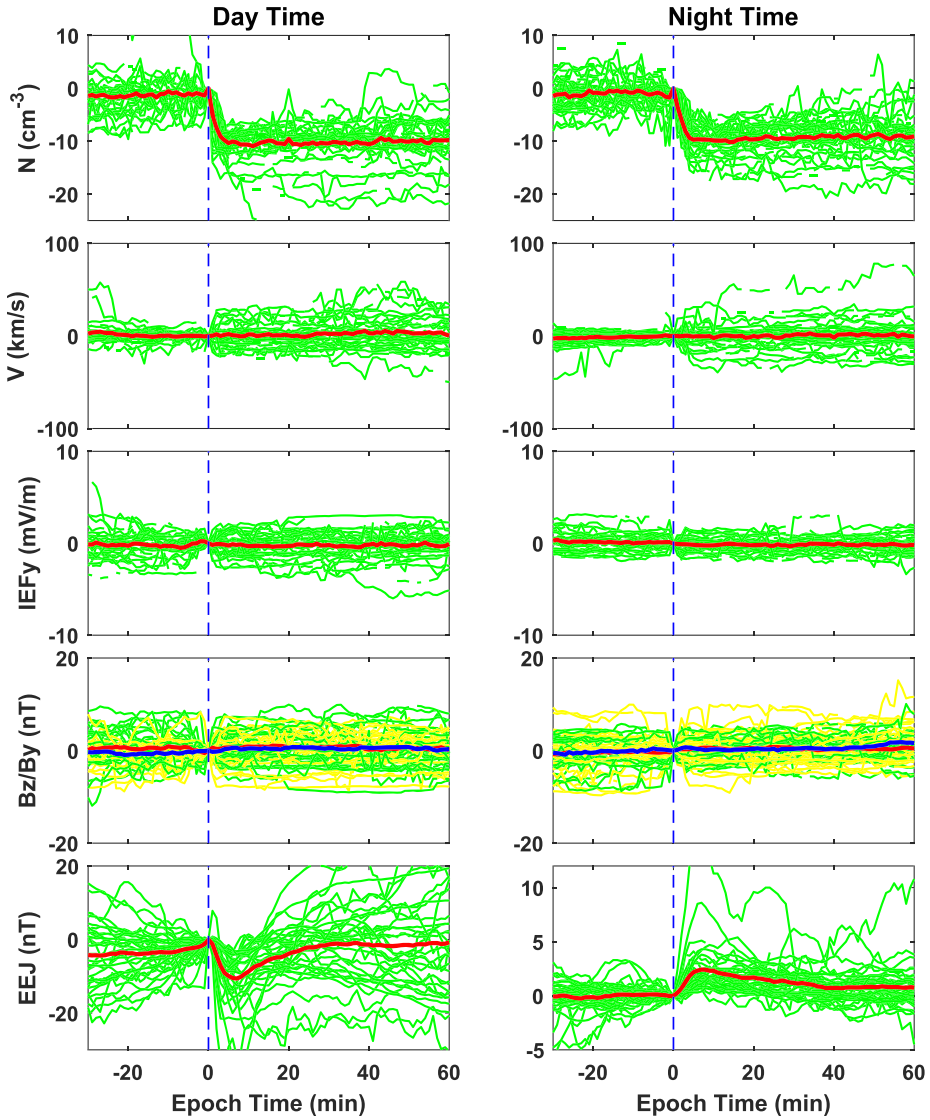

Figure 6. Same as Figure 3 except for the cases of sharp decreases in the solar wind density.

EEJ depends on both σ_c and E_x. Therefore, the sharp increases/decreases in EEJ observed in Figures 1 and 4 are mainly due to the prompt eastward/westward disturbances in the ionospheric electric field (E_x) on dayside/nightside, respectively. This satisfies the curl-free condition of ionospheric electric fields. The significantly smaller EEJ changes on nightside are further affirmative of electric field disturbances in ionosphere and the resultant currents on the nightside are smaller compared to dayside due to the very low ionospheric conductivity on the nightside.

Huang et al. (2008) have shown the similar prompt enhancements in the geomagnetic field and eastward electric field disturbances (vertical $E \times B$ drifts) on dayside from the Jicamarca incoherent scatter radar in response to the sudden enhancements in the P_{Dyn}. Huang et al. (2008) have also shown the enhanced high-latitude ionospheric convection in response to P_{Dyn} shock. They have discussed about the two possible mechanisms driven by (i) P_{Dyn} shock causing over compression of magnetosphere and enhanced magnetopause currents and (ii) enhanced field-aligned currents and ionospheric currents. While the simultaneous enhancement of magnetopause currents, field-aligned currents, and ionospheric currents are necessary, Huang et al. (2008) have concluded that neither of the above two mechanisms can fully explain the observed changes in the geomagnetic field and electric field disturbances. Later, Wei et al. (2012) have shown the

coherent variation of cross polar cap potential (CPCP) in response to the solar wind density changes under saturated polar cap conditions during a super geomagnetic storm of November 2003. While they conclude that the full physical picture on the relationship between the solar wind density and PPEF cannot be clearly identified, they, however, mentioned about the roles of parameters such as P_{Dyn}, Alfven Mach number and plasma beta parameters (e.g., Lopez et al., 2004; Wilder et al., 2009). Yu and Ridley (2011) also observed that the cross polar cap potential changes considerably in the first few minutes after solar wind density enhancement.

Lopez et al. (2004) have carried out MHD simulations under strong southward IMF (−20 nT) conditions and found that the magnetic field (IMF) compression ratio across the low Mach number bow shock is strongly affected by the solar wind density. A higher compression ratio across the bow shock causes greater amount of magnetic energy is available in the magnetosheath. Thus, a stronger solar wind magnetic field is available at magnetopause reconnection causing increased reconnection rate and high-latitude convection as well as CPCP. However, this mechanism cannot explain the brief pulse-like variation of EEJ in response to the step-like increase of density which remains at high levels for several tens of minutes. Ober et al. (2007) have also shown, through MHD simulations, the transient pulse-like polar cap potential increase/decrease for ~25–30 min period in response to the sudden increase/decrease in the solar wind density, respectively. They have interpreted the increased polar cap potential as a result of erosion of dayside closed magnetic flux via enhanced (dayside) merging rate in response to the magnetospheric fast compression wave driven by sudden density enhancement. Similarly, the decrease of polar cap potential is caused by the decrease in dayside merging rate to accommodate the needed accumulation of closed magnetic flux during the expansion of magnetosphere due to fast rarefaction wave driven by the sudden decrease in density (Ober et al., 2007). The increase/decrease of polar cap potential indicates the enhancement/reduction in the high-latitude convection electric fields, respectively. However, the increase/decrease in dayside merging rate in response to sudden increase/decrease shown by Ober et al. (2007) are under strong southward IMF *Bz* (−12 nT) conditions. The dayside merging rate either due to greater amount of magnetosheath fields (Lopez et al., 2004) or via dayside magnetic flux erosion (Ober et al., 2007) is expected to significantly enhance under southward IMF *Bz* conditions. In fact, both the above simulations studies are carried under strong southward IMF *Bz* conditions. However, the dayside merging rate is not expected significantly enhance under northward IMF *Bz* conditions (except a minor contribution from high-latitude lobe reconnection). It should be noted here that the events of sharp density enhancements and reductions presented in Figures 3 and 6 correspond to different background IMF *Bz* and *By* conditions. Nevertheless, the corresponding response of EEJ consistently indicates the eastward (westward) PPEF in the dayside (nightside) for the cases of density enhancements (Figure 3) irrespective of the background *Bz* and *By* conditions. Similarly, the opposite responses of EEJ have found consistently for the cases of sharp density reductions (Figure 6) without any clear dependency of the background IMF *Bz* and *By* conditions. It should also be mentioned here that the IMF *Bz* and *By* often found to exhibit small fluctuations and/or deflections along with the sharp density enhancements/reductions shown in Figures 3 and 6. One may recall that these changes in IMF *Bz* and *By* are only small (i.e., $|\Delta Bz|_{10min} < 10$ nT and $|\Delta By|_{10min} < 10$ nT) because of our selection criteria for the events mentioned in the previous section. However, with a view to further examine the effects of these small IMF *Bz* variations on the PPEF disturbances during the sharp solar wind density changes, the events presented in the Figures 3 and 6 are further classified in to (i) slightly northward deflecting IMF *Bz* ($1 \text{ nT} \leq \Delta Bz_{10min} < 10$ nT), (ii) slightly southward deflecting IMF *Bz* ($-1 \text{ nT} \geq \Delta Bz_{10min} > -10$ nT), and (iii) nearly steady IMF *Bz* (ΔBz_{10min} within ±1 nT) conditions during the 10 min period from the time of sudden change in density (within 0 to 10 min epoch time). Figures 7a and 7b (top panels) show the changes observed in EEJ (ΔEEJ) in response to the sharp density enhancements and reductions, respectively, as a function of local time. Here, the ΔEEJ is defined as the maximum positive/negative excursion of EEJ within 10 min from the time of sudden change in the density (i.e., within zero to 10 min epoch time). The red and blue circles represent the cases where the ΔBz_{10min} is southward ($-1 \text{ nT} \geq \Delta Bz_{10min} > -10$ nT) and northward ($1 \text{ nT} \leq \Delta Bz_{10min} < 10$ nT), respectively. Whereas the black circles represent the cases where the IMF *Bz* is nearly steady (i.e., ΔBz_{10min} within ±1 nT). It can be clearly seen from these figures that the EEJ response is positive and negative during daytime and nighttime periods, respectively, for density enhancements (left panel). Similarly, the EEJ response is negative and positive during daytime and nighttime periods, respectively, for density reductions (right panels). However, the magnitude of EEJ response during

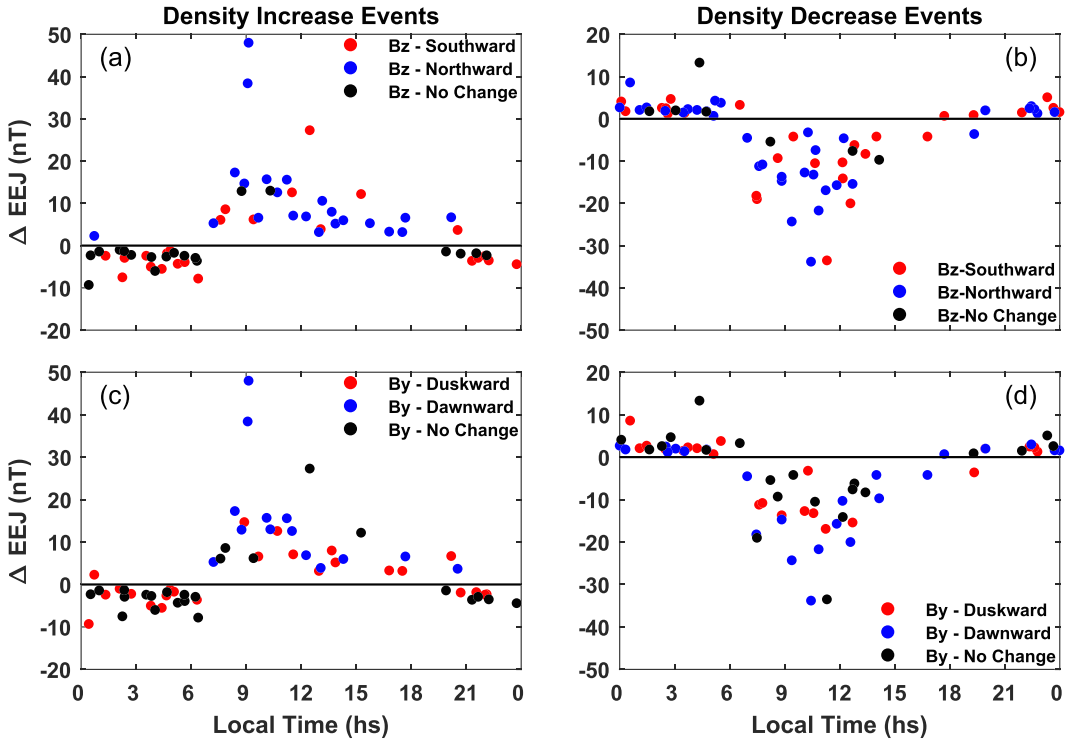

Figure 7. Changes observed in EEJ (ΔEEJ) in response to the sharp density enhancements (a, c) and reductions (b, d) as a function of local time. The red and blue solid circles in the top panels (bottom panels) represent the cases where the IMF *Bz* (*By*) exhibited small southward (duskward) and northward (dawnward) deflections, respectively, during the time of sharp change in the density (i.e., 0 to 10 min epoch time). The black solid circles represent the cases when the IMF *Bz* or *By* are steady. Please refer to text for more details.

nighttime periods is significantly smaller compared to daytime periods as the ionospheric conductivity is very low during nighttimes. The interesting observation from Figures 7a and 7b is that the polarity of electric fields disturbances (or EEJ changes) depend mainly on the local time without any dependence on the these small IMF *Bz* changes at the time of density changes. In other words, the present results show eastward (westward) PPEF on dayside (nightside) consistently occurred in response to sharp density enhancements irrespective of small southward/northward deflections in IMF *Bz*. Huang et al. (2008) also showed the similar enhancements in vertical ion ($E \times B$) drift velocities on the dayside in response to P_{Dyn} shocks irrespective of IMF *Bz* polarity. Similar analysis is carried out to examine the effects of small IMF *By* variations occurred during these events, as shown in Figures 7c and 7d (bottom panels). As can be seen from these figures, the polarity of PPEF disturbances mainly depends on the local time without any clear dependence on the smaller changes that occurred in IMF *By*. Hence, from the results presented in Figure 7, one can conclude that the observed PPEF disturbances in EEJ are mainly due to the sharp changes in the solar wind density without any clear effects due to the smaller changes in IMF *Bz* and *By*.

Araki (1994) has explained the ground magnetic field responses to geomagnetic SC as a combination of disturbance low-latitude (DL) and disturbance polar (DP) fields. The sudden increase of P_{Dyn} caused by enhancement of density and/or velocity causes the increased magnetopause currents and also launches a compressional hydromagnetic (HM) wave propagating toward Earth. The *H* component of ground magnetic field increases during the passage of this compressional wavefront of finite thickness. The combined effects of magnetopause currents and compressional wave give rises to a sharp step-like enhancement of geomagnetic field at low latitudes, so called DL component. While the compressional wavefront is propagating toward Earth, the inhomogeneity of plasma and magnetic field in the magnetosphere causes transverse mode Alfven wave propagation and produces a current component along the field lines to high-latitude ionosphere accompanied with dusk-to-dawn electric field (Tamao, 1964). This high-latitude dusk-to-dawn electric field may penetrate to low latitudes nearly with a velocity light by the zeroth order transverse

magnetic (TM) mode in the Earth-ionosphere waveguide (Kikuchi et al., 1978). When this Alfven wave mode disturbance in the electric field is larger than the positive compressional wave, a brief impulse of ~1–2 min duration with negative and positive polarities can be observed, known as preliminary reverse impulse (PRI) and preliminary positive impulse (PPI) depending on local time and latitude of the location (Araki, 1994; Kikuchi & Araki, 1985).

Even after the passage of fast mode compressional wave, the enhanced solar wind dynamic pressure (due to elevated density in the present case) behind the shock leads to the new compressed state of magnetosphere. The compression due to the elevated solar wind density levels also causes the earthward flow of dayside magnetospheric plasma through viscous interaction (Axford & Hines, 1961). The viscous-like interaction enhances the plasma flow parallel to the magnetopause. Hence, the velocity of plasma flow will be larger near the magnetopause and magnetospheric flanks; and reduces as it moves toward the inner magnetosphere. This gradient in the plasma flow can induce flow shear in the dayside magnetosphere. Fujita et al. (2003) and Kubota et al. (2015) have actually shown (through MHD simulations) the antisunward propagating plasma flow shear near the magnetospheric flanks and termed it as "Transit Cell Convection". The velocity shear drives field-aligned currents from dayside magnetosphere that flow into dawn ionosphere and out from the dusk ionosphere, that is, in the same directional sense as Region 1 currents (Fujita et al., 2003; Kubota et al., 2015). This transit cell convection is excited within the magnetosphere by the compression of magnetospheric flanks and gradually decay in about ~20 min as the magnetospheric plasma flow slowly adjusted to the new compressed state. Araki (1977, 1994) has also mentioned that the convection should increase in order to adjust the new compressed state of magnetosphere during MI and the associated field-aligned currents from dayside magnetosphere flow into dawn ionosphere and out from the dusk ionosphere. It should be noted that this convection is mainly driven by the compression of dayside magnetosphere and can occur under both northward and southward IMF *Bz* conditions. In fact, the transit cell convection shown through MHD simulation by Fujita et al. (2003) is carried out under northward IMF *Bz* (4.33 nT) conditions. However, the convection can significantly enhance during southward IMF *Bz* conditions due to enhanced dayside merging rate (e.g., Lopez et al., 2004; Ober et al., 2007; Wei et al., 2012). The resultant dawn-to-dusk electric field penetrates promptly to low latitudes and causes sharp PPEF disturbances of ~10–20 min (Araki, 1994; Kikuchi et al., 2001) and up to ~1 hr (Sastri, 2002) periods, known as MI. Therefore, the low-latitude response during the sudden enhancement of P_{Dyn} (and/or density) is the combination of PPEF fields due to PI (DP_{PI}) and MI (DP_{MI}) superimposed on step-like increase due to DL. While the current source for DL remains in the magnetosphere, the DP_{PI} and DP_{MI} are due to currents flowing in the ionosphere. Further, the ionospheric currents associated with DP_{PI} and DP_{MI} exhibit equatorial enhancements due to Cowling effect (Hirono, 1952). Since the contributions from DL will be more or less removed by subtracting the low-latitude geomagnetic field variations (ΔH at Alibag) from the equatorial field variations (ΔH at Alibag), the resultant EEJ variations mainly represent the PPEFs due to PI and MI. However, the brief ~1 min impulses due to PRI/PI are not consistently observed in the present observations, which can be partly due to low (1-min) resolution of magnetometer data considered in this analysis. On the other hand, the pulse-like EEJ perturbations of ~20 min periods agree with the penetration of dawn-to-dusk electric field associated with MI. The dawn-to-dusk electric field is eastward in the dayside and westward in the nightside, causing opposite responses of EEJ to the solar wind density enhancement, as shown in the present analysis. Therefore, the present study further confirms the penetration of dawn-to-dusk convection electric field to equatorial altitudes in response to sudden enhancements in solar wind density alone without any significant changes in the velocity and IEFy. Further, this study also showcases the PPEFs of opposite polarity in response to sharp reduction in the density, probably due to sudden reduction in convection electric fields in order to adjust for the rarefied state of magnetosphere (Araki & Nagano, 1988; Hori et al., 2015).

5. Conclusions

A systematic statistical study is carried out using long-term (2001–2018) observations of equatorial electrojet over the Indian sector to investigate the role of solar wind density on the prompt equatorial electric field disturbances. The events of sharp solar wind density enhancements/decreases without significant changes in the other solar wind parameters (such as velocity, IMF *Bz*, *By*, and IEFy) have been selected to study the exclusive control of solar wind density on the PPEF disturbances in the equatorial ionosphere. It is found that the EEJ exhibits prompt increase (decrease) indicating the prompt eastward

(westward) electric field disturbances in the dayside (nightside) equatorial ionosphere in response to the sudden enhancements in the solar wind density. While the density exhibits a step-like increase (remains to be high for several minutes after the increase), the responsive EEJ exhibits a spiky pulse-like variation (sharp rise and fall) of ~20 min duration. Similar EEJ disturbances of opposite polarity have also been observed in response to the sudden decrease of solar wind density. Further, the polarity of observed changes in EEJ or equatorial electric field disturbances depends mainly on the local time and are independent of the background IMF *Bz* and *By* conditions and their small variations. The responsible mechanisms for the observed EEJ disturbances can be attributed to the enhanced magnetospheric convection for about ~20 min in response to sudden increase in solar wind pressure/density and the penetration of dawn-to-dusk electric fields to low-latitudes.

Data Availability Statements

The SuperDARN convection map data are obtained from this site (http://vt.superdarn.org/tiki-index.php?page=Conv+map+overview). The magnetometer data of Tirunelveli and Alibag can be obtained from World Data Centre for Geomagnetism, Mumbai at this site (http://www.wdciig.res.in/).

Acknowledgments

This work is supported by Department of Science and Technology, Government of India, and ISEE, Nagoya University under ISEE international joint research program (2019–2020). The work of K. Shiokawa is supported by JSPS KAKENHI (15H05815 and 16H06286), and the work of N. Balan is supported by the National Key R&D Program of China (2018YFC1407304 and 2018YFC1407303). The open data policy of Space Physics Data Facility (SPDF), NASA, USA (https://omniweb.gsfc.nasa.gov/ow_min.html) for the solar wind data is duly acknowledged.

References

Abdu, M. A., Batista, I. S., Walker, G. O., Sobral, J. H. A., Trivedi, N. B., & de Paula, E. R. (1995). Equatorial ionospheric fields during magnetospheric disturbances: Local time/longitudinal dependences from recent EITS campaigns. *Journal of Atmospheric and Solar - Terrestrial Physics*, *57*(10), 1065–1083. https://doi.org/10.1016/0021-9169(94)00123-6

Anderson, D., Anghel, A., Yumoto, K., Ishitsuka, M., & Kudeki, E. (2002). Estimating daytime vertical E × B drift velocities in the equatorial F region using ground-based magnetometer observations. *Geophysical Research Letters*, *29*(12), 1596. https://doi.org/10.1029/2001GL014562

Araki, T. (1977). Global structure of geomagnetic sudden commencements. *Planetary and Space Science*, *25*(4), 373–384. https://doi.org/10.1016/0032-0633(77)90053-8

Araki, T. (1994). A physical model of the geomagnetic sudden commencement. In M. J. Engebretson, K. Takahashi, & M. Scholer (Eds.), *Solar wind sources of magnetospheric ultra-low-frequency waves* (pp. 183–200). Washington, DC: AGU.

Araki, T., & Nagano, H. (1988). Geomagnetic response to sudden expansions of the magnetosphere. *Journal of Geophysical Research*, *93*(A5), 3983–3988. https://doi.org/10.1029/JA093iA05p03983

Axford, W. I., & Hines, C. O. (1961). A unifying theory of high-latitude geophysical phenomena and geomagnetic storms. *Canadian Journal of Physics*, *39*(10), 1433–1464. https://doi.org/10.1139/p61-172

Basu, S., Basu, S., Groves, K. M., MacKenzie, E., Keskinen, M. J., & Rich, F. J. (2005). Near-simultaneous plasma structuring in the mid-latitude and equatorial ionosphere during magnetic superstorms. *Geophysical Research Letters*, *32*, L12S05. https://doi.org/10.1029/2004GL021678

Basu, S., Basu, S., Groves, K. M., Yeh, H. C., Su, S. Y., Rich, F. J., et al. (2001). Response of the equatorial ionosphere in the South Atlantic region to the great magnetic storm of July 15, 2000. *Geophysical Research Letters*, *28*(18), 3577–3580. https://doi.org/10.1029/2001GL013259

Chakrabarty, D., Hui, D., Rout, D., Sekar, R., Bhattacharyya, A., Reeves, G. D., & Ruohoniemi, J. M. (2017). Role of IMF by in the prompt electric field disturbances over equatorial ionosphere during a space weather event. *Journal of Geophysical Research: Space Physics*, *122*, 2574–2588. https://doi.org/10.1002/2016JA022781

Ebihara, Y., Tanaka, T., & Kikuchi, T. (2014). Counter equatorial electrojet and overshielding after substorm onset: Global MHD simulation study. *Journal of Geophysical Research: Space Physics*, *119*, 7281–7296. https://doi.org/10.1002/2014JA020065

Fejer, B. G. (1991). Low-latitude electrodynamic plasma drifts: A review. *Journal of Atmospheric and Terrestrial Physics*, *53*(8), 677–693. https://doi.org/10.1016/0021-9169(91)90121-M

Fejer, B. G., & Scherliess, L. (1997). Empirical models of storm time equatorial zonal electric fields. *Journal of Geophysical Research*, *102*(A11), 24,047–24,056. https://doi.org/10.1029/97JA02164

Fujita, S., Tanaka, T., Kikuchi, T., Fujimoto, K., & Itonaga, M. (2003). A numerical simulation of the geomagnetic sudden commencement: 2. Plasma processes in the main impulse. *Journal of Geophysical Research*, *108*(A12), 1417. https://doi.org/10.1029/2002JA009763

Hashimoto, K. K., Kikuchi, T., Tomizawa, I., & Nagatsuma, T. (2017). Substorm overshielding electric field at low latitude on the nightside as observed by the HF Doppler sounder and magnetometers. *Journal of Geophysical Research: Space Physics*, *122*, 10,851–10,863. https://doi.org/10.1002/2017JA024329

Hirono, M. (1952). A theory of diurnal magnetic variations in equatorial regions and conductivity of the ionosphere E region. *Journal of Geomagnetism and Geoelectricity*, *4*(1), 7–21. https://doi.org/10.5636/jgg.4.7

Hori, T., Shinbori, A., Fujita, S., & Nishitani, N. (2015). IMF-*By* dependence of transit ionospheric flow perturbation associated with sudden impulses: SuperDARN observations. *Earth, Planets and Space*, *67*(1), 190. https://doi.org/10.1186/s40623-015-0360-6

Huang, C.-S. (2012). Statistical analysis of dayside equatorial ionospheric electric fields and electrojet currents produced by magnetospheric substorms during sawtooth events. *Journal of Geophysical Research*, *117*, A02316. https://doi.org/10.1029/2011JA017398

Huang, C.-S., Foster, J. C., Goncharenko, L. P., Reeves, G. D., Chau, J. L., Yumoto, K., & Kitamura, K. (2004). Variations of low-latitude geomagnetic fields and Dst index caused by magnetospheric substorms. *Journal of Geophysical Research*, *109*, A05219. https://doi.org/10.1029/2003JA010334

Huang, C.-S., Yumoto, K., Abe, S., & Sofko, G. (2008). Low-latitude ionospheric electric and magnetic field disturbances in response to solar wind pressure enhancements. *Journal of Geophysical Research*, *113*, A08314. https://doi.org/10.1029/2007JA012940

Kane, R. P. (1974). Relation between the strength of the Sq current system and its focus position. *Proceedings of the Indian Academy of Sciences*, *A80*, 17–25.

Kelley, M. C., Fejer, B., & Gonzales, C. (1979). An explanation for anomalous equatorial ionospheric electric fields associated with a northward turning of the interplanetary magnetic field. *Geophysical Research Letters*, *6*(4), 301–304. https://doi.org/10.1029/GL006i004p00301

Kelley, M. C., & Makela, J. J. (2002). By dependent prompt penetrating electric fields at the magnetic equator. *Geophysical Research Letters*, *29*(7), 1153. https://doi.org/10.1029/2001GL014468

Kikuchi, T. (1986). Evidence of transmission of polar electric fields to the low latitude at times of geomagnetic sudden commencements. *Journal of Geophysical Research*, *91*, 3101.

Kikuchi, T., & Araki, T. (1985). Preliminary positive impulse of geomagnetic sudden commencement observed at dayside middle and low latitudes. *Journal of Geophysical Research*, *90*(A12), 12,195–12,200. https://doi.org/10.1029/JA090iA12p12195

Kikuchi, T., Araki, T., Maeda, H., & Maekawa, K. (1978). Transmission of polar electric fields to the equator. *Nature*, *273*(5664), 650–651. https://doi.org/10.1038/273650a0

Kikuchi, T., Hashimoto, K. K., Kitamura, T. I., Tachihara, H., & Fejer, B. J. (2003). Equatorial counter electrojets during substorms. *Journal of Geophysical Research*, *108*(A11), 1406. https://doi.org/10.1029/2003JA009915

Kikuchi, T., Ishimine, T., & Sugiuchi, H. (1985). Local time distribution of HF Doppler frequency deviations associated with geomagnetic storm sudden commencements. *Journal of Geophysical Research*, *90*, 4389.

Kikuchi, T., Luhr, H., Kitamura, T., Saka, O., & Schlegel, K. (1996). Direct penetration of the polar electric fields to the equator during a DP 2 event as detected by the auroral and equatorial magnetometer chains and the EISCAT radar. *Journal of Geophysical Research*, *101*(A8), 17,161–17,173. https://doi.org/10.1029/96JA01299

Kikuchi, T., Luhr, H., Schlegel, K., Tachihara, H., Shinohara, M., & Kitamura, T. L. (2000). Penetration of auroral electric fields to the equator during a substorm. *Journal of Geophysical Research*, *105*(A10), 23,251–23,261. https://doi.org/10.1029/2000JA900016

Kikuchi, T., Tsunomura, S., Hashimoto, K., & Nozaki, K. (2001). Field-aligned current effects on mid-latitude geomagnetic sudden commencements. *Journal of Geophysical Research*, *106*(A8), 15,555–15,565. https://doi.org/10.1029/2001JA900030

Kubota, Y., Kataoka, R., Den, M., Tanaka, T., Nagatsuma, T., & Fujita, S. (2015). Global MHD simulation of magnetospheric response of preliminary impulse to large and sudden enhancement of the solar wind dynamic pressure. *Earth, Planets and Space*, *67*(1), 94. https://doi.org/10.1186/s40623-015-0270-7

Lopez, R. E., Wiltberger, M., Hernandez, S., & Lyon, J. G. (2004). Solar wind density control of energy transfer to the magnetosphere. *Geophysical Research Letters*, *31*, L08804. https://doi.org/10.1029/2003GL018780

Nishida, A. (1968). Coherence of geomagnetic DP2 fluctuations with interplanetary magnetic variations. *Journal of Geophysical Research*, *73*(17), 5549–5559. https://doi.org/10.1029/JA073i017p05549

Ober, D. M., Wilson, G. R., Burke, W. J., Maynard, N. C., & Siebert, K. D. (2007). Magnetohydrodynamic simulations of transient transpolar potential responses to solar wind density changes. *Journal of Geophysical Research*, *112*, A10212. https://doi.org/10.1029/2006JA012169

Pudovkin, M. I., Besser, B. P., & Zaitseva, S. A. (1998). Magnetopause stand-off distance in dependence on the magnetosheath and solar wind parameters, Ann. *Geophysica*, *16*(4), 388–396. https://doi.org/10.1007/s00585-998-0388-z

Rastogi, R. G. (1977). Geomagnetic storms and electric fields in the equatorial ionosphere. *Nature*, *268*(5619), 422–424. https://doi.org/10.1038/268422a0

Rastogi, R. G., Chandra, H., & James, M. E. (1996). Nocturnal variations of geomagnetic horizontal field at equatorial stations. *Geophysical Research Letters*, *23*(19), 2601–2604. https://doi.org/10.1029/96GL02390

Rastogi, R. G., & Patel, V. L. (1975). Effect of interplanetary magnetic field on ionosphere over the magnetic equator. *Proceedings of the Indian Academy of Sciences-Section A*, *82*(4), 121–141. https://doi.org/10.1007/BF03046722

Reddy, C. A. (1989). The equatorial electrojet. *Pure and Applied Geophysics*, *131*(3), 485–508. https://doi.org/10.1007/BF00876841

Rout, D., Chakrabarty, D., Sekar, R., Reeves, G. D., Ruohoniemi, J. M., Pant, T. K., et al. (2016). An evidence for prompt electric field disturbance driven by changes in the solar wind density under northward IMF *Bz* condition. *Journal of Geophysical Research: Space Physics*, *121*, 4800–4810. https://doi.org/10.1002/2016JA022475

Sastri, J., Rao, J., Rao, D., & Pathan, B. (2001). Daytime equatorial geomagnetic H field response to the growth phase and expansion phase onset of isolated substorms: Case studies and their implications. *Journal of Geophysical Research*, *106*(A12), 29,925–29,933. https://doi.org/10.1029/2001JA900120

Sastri, J. H. (2002). Penetration electric fields at the nightside dip equator associated with the main impulse of the storm sudden commencement of 8 July 1991. *Journal of Geophysical Research*, *107*(A12), 1448. https://doi.org/10.1029/2002JA009453

Sastri, J. H., Rao, J. V. S. V., & Ramesh, K. B. (1993). Penetration of polar electric fields to the nightside dip equator at times of geomagnetic sudden commencements. *Journal of Geophysical Research*, *98*(A10), 17,517–17,523. https://doi.org/10.1029/93JA00418

Senior, C., & Blanc, M. (1984). On the control of magnetospheric convection by the spatial distribution of ionospheric conductivities. *Journal of Geophysical Research*, *89*(A1), 261–284. https://doi.org/10.1029/JA089iA01p00261

Tamao, T. (1964). The structure of three-dimensional hydromagnetic waves in a uniform cold plasma. *Journal of Geomagnetism and Geoelectricity*, *18*, 89–114.

Tulasi Ram, S., Balan, N., Veenadhari, B., Gurubaran, S., Ravindran, S., Tsugawa, T., et al. (2012). First observational evidence for opposite zonal electric fields in equatorial *E* and *F* region altitudes during a geomagnetic storm period. *Journal of Geophysical Research*, *117*, A09318. https://doi.org/10.1029/2012JA018045

Tulasi Ram, S., Nilam, B., Balan, N., Zhang, Q., Shiokawa, K., Chakrabarty, D., et al. (2019). Three different episodes of prompt equatorial electric field perturbations under steady southward IMF *Bz* during St. Patrick's Day storm. *Journal of Geophysical Research: Space Physics*, *124*, 10,428–10,443. https://doi.org/10.1029/2019JA027069

Tulasi Ram, S., RamaRao, P. V. S., Prasad, D. S. V. V. D., Niranjan, K., GopiKrishna, S., Sridharan, R., & Ravindran, S. (2008). Local time dependent response of post-sunset ESF during geomagnetic storms. *Journal of Geophysical Research*, *113*, A07310. https://doi.org/10.1029/2007JA012922

Tulasi Ram, S., Yokoyama, T., Otsuka, Y., Shiokawa, K., Sripathi, S., Veenadhari, B., et al. (2015). Duskside enhancement of equatorial zonal electric field response to convection electric fields during the St. Patrick's Day storm on 17 march 2015. *Journal of Geophysical Research: Space Physics*, *121*, 538–548. https://doi.org/10.1002/2015JA021932

Venkatesh, K., Tulasi Ram, S., Fagundes, P. R., Seemala, G. K., & Batista, I. S. (2017). Electrodynamic disturbances in the Brazilian equatorial and low-latitude ionosphere on St. Patrick's Day storm of 17 march 2015. *Journal of Geophysical Research: Space Physics*, *122*, 4553–4570. https://doi.org/10.1002/2017JA024009

Wei, Y., Wan, W., Zhao, B., Hong, M., Ridley, A., Ren, Z., et al. (2012). Solar wind density controlling penetration electric field at the equatorial ionosphere during a saturation of cross polar cap potential. *Journal of Geophysical Research*, *117*, A09308. https://doi.org/10.1029/2012JA017597

Wilder, F. D., Clauer, C. R., & Baker, J. B. H. (2009). Reverse convection potential saturation during northward IMF under various driving conditions. *Journal of Geophysical Research*, *114*, A08209. https://doi.org/10.1029/2009JA014266

Yu, Y. Q., & Ridley, A. J. (2011). Understanding the response of the ionosphere-magnetosphere system to sudden solar wind density increases. *Journal of Geophysical Research*, *116*, A04210. https://doi.org/10.1029/2010JA015871

Yuan, Z., & Deng, X. (2007). Effects of continuous solar wind pressure variations on the long-lasting penetration of interplanetary electric field during southward interplanetary magnetic field. *Advances in Space Research*, *39*(8), 1342–1346. https://doi.org/10.1016/j.asr.2007.02.033